Distribution of Magnetic Moment in Metallic Gadolinium†

R. M. Moon, W. C. Koehler, J. W. Cable, and H. R. Child
Solid State Division, Oak Ridge National Laboratory, Oak Ridge, Tennessee 37830
(Received 23 August 1971)

Neutron-diffraction experiments with both polarized and unpolarized neutrons have been carried out on single-crystal specimens of ^{160}Gd in order to measure the magnetic-moment distribution in the metal. Data have been obtained in the ferromagnetic state at 96 °K for all $(hk0)$ reflections out to $(\sin\theta)/\lambda = 1.275$ and nearly all $(0kl)$ peaks to $(\sin\theta)/\lambda = 1.04$. Measurements have been made as well at a temperature above the Curie point. The shape of the spin distribution appears to be identical at the elevated temperature (313 °K) to that observed at 96 °K. The form-factor data can logically be separated into diffuse and localized components, which may be identified with the conduction electrons and $4f$ electrons, respectively. The $4f$ density is spherically symmetric, and it has a radial dependence which is significantly expanded relative to Hartree-Fock wave functions for the free trivalent ion. Good agreement can be achieved with theoretical form factors based on relativistic Hartree-Fock-Slater wave functions. The diffuse density does not have the distribution expected for $5d$ or $6s$ orbitals: It is long range and oscillatory, however, as one expects for conduction electrons in the rare earths. Measurements of the form factor of Gd^{+3} in paramagnetic Gd_2O_3 have also been made, and the results are in excellent agreement with the free-ion calculations, except at very small scattering angles.

I. INTRODUCTION

In many respects gadolinium is one of the simplest magnetic materials known. As such it would be an ideal candidate for a number of neutron-scattering experiments, except for the extremely high thermal-neutron-capture cross section of the naturally occurring element. This difficulty has recently been overcome by the production, in this laboratory, of metal highly enriched in the low-capturing isotope ^{160}Gd. In this paper we report the results of precision measurements, with both polarized and unpolarized neutrons, of the magnetic-scattering amplitude of gadolinium measured on single-crystal samples of the isotopically enriched metal.

Gadolinium behaves magnetically as if it contained tripositive ions in $^8S_{7/2}$ states: The outer $5d$ and $6s$ electrons of the free atom form the conduction band. From paramagnetic-susceptibility measurements[1] in the temperature range 400–900 °K, an effective moment of $(7.98 \pm 0.05)\mu_B$ was deduced which is in good agreement with the theoretical value $\mu_{\text{eff}} = g[J(J+1)]^{1/2} = 7.94\mu_B$, with $g = 2.0$ and $J = S = \frac{7}{2}$.

Below its Curie point of 293.2 °K, gadolinium is a simple ferromagnet. The easy direction of spontaneous magnetization varies with temperature in a complex manner[2–4] but, because the atoms are in S states, the anisotropy energy is relatively low and it is possible to achieve magnetic saturation in a number of directions in the crystal with relatively weak fields. For application of the polarized beam technique this is an important consideration.

At 4.2 °K, the measured saturation magnetization corresponds to $7.55\mu_B$/atom,[1] a value which is $0.55\mu_B$ in excess of $7.0\mu_B$ due to seven electrons in the half-filled $4f$ shell. This excess moment is usually attributed to polarization of the conduction-electron system.

The polarized-beam technique has been used with great success to determine the magnetic form factors of ferromagnetic elements and alloys of the $3d$ transition series. By Fourier inversion one obtains direct information on the spatial distribution of the periodic magnetic-moment density, but considerable analysis is then required to extract information about the distribution of the $3d$ electrons.[5] The technique has recently been applied to the rare-earth metals Tb[6,7] and Tm,[8] but, because of the high anisotropy and the large spin-orbit coupling in these metals, only a limited amount of data is obtainable. The analysis is further complicated by deviations from spherical symmetry of the charge and current distributions in the metals. In gadolinium, however, the magnetic-moment density is proportional to the unpaired spin density.

The aim of this experiment has been to measure the $4f$ spin distribution and to learn something of the nature of the conduction-electron distribution. That this aim has been realized has been reported briefly earlier[9–11]; we give here a detailed description of the experiments, and of the analysis leading to the separation of $4f$ and conduction-electron distributions. Throughout the analysis the assumption is made that the spin density is collinear so that it can be described by a scalar density function.

Measurements were made as well on metallic gadolinium at 313 °K, at which temperature a moment was induced by the application of an external field, and on isotopically enriched paramagnetic

TABLE I. Properties of the specimen crystals.

Crystal	1	2	3
Length (cm)	0.859	0.610	1.016
Cross section (cm)	0.041×0.058	0.0610×0.102	0.211×0.244
Figure axis	c	a	c
η[a] (rad)	0.0027±0.0014	0.0019±0.0006	0.0013±0.0002

[a]Full width at half-maximum of the mosaic distribution equals $2(2\ln 2)^{1/2}\eta$.

Gd_2O_3. Information on the temperature dependence of the unpaired spin-density distribution and on the comparison of metallic and ionic form factors was sought in these experiments. Results are given in the appropriate sections of the text.

II. EXPERIMENTAL DETAILS

A. Sample Properties

A button of some 40 g of metal enriched to 99.993% ^{160}Gd was prepared from oxide separated by the Stable Isotopes Division of this laboratory. With a modification of the strain-anneal process reported by Nigh[12] several large grains were produced in the button from which neutron-diffraction specimens were cut. Three crystals were investigated; a number of pertinent properties of the specimens are listed in Table I. Crystals 1 and 2 were used in both the polarized and unpolarized beam experiments. The total neutron cross section of the metal at 70 meV was found to be 20.3 b.

To avoid loss of the isotopic sample, chemical analyses were not performed on it. Analyses were carried out, however, on a specimen of metal of normal isotopic constitution which had been subjected to the same operations. The following impurities in ppm were detected: Ca ≃ 100; Mg < 100; Fe < 200; Ta ≃ 1000; Y < 50; Tb < 500; Dy < 1000; Ho < 200; Cu < 100; O_2 ≃ 1600; N_2 ≃ 100, and these may be considered representative of the isotopic sample as well.

At room temperature Gd crystallizes in the simple hexagonal closepacked structure with $a = 3.636$ Å and $c = 5.783$ Å. Below the Curie point the c axis exhibits an anomalous expansion, whereas the a dimension shows normal lattice contraction. The measurements by Darnell[13] on the temperature dependence of the lattice constants were used in setting up our experiments.

B. Apparatus and Procedure

All the measurements were made at the HB-1 triple-axis spectrometer at the high-flux isotope reactor (HFIR). The metallic specimens were mounted in a "cold-finger"-type cryostat designed so that the specimen could be rotated about its figure axis by means of external controls. With liquid nitrogen in the cryostat the samples reached an equilibrium temperature of 96 °K. A magnetic field of 12.5 kOe was applied normal to the scattering plane and parallel to the figure axis of the specimen.

The polarized-beam technique yields, in principle, the so-called flipping ratio

$$R = \frac{(1+p/b)^2}{(1-p/b)^2}, \tag{1}$$

where p and b are the magnetic- and nuclear-scattering amplitudes, respectively. The magnetic-scattering amplitude $p = p_0 \mu f$, where p_0 is a well-known constant ($e^2\gamma/2mc^2$), μ is the magnetic moment in Bohr magnetons, and f is the normalized form factor. The method gives highly precise results when $p/b \ll 1$, for in this case R is relatively insensitive to instrumental imperfections and beam depolarization. When $p \approx b$, such corrections become very important, and have to be determined with great accuracy. When $p \gg b$, the flipping ratio is less sensitive to p than for $p \ll b$ but the method is nevertheless capable, with care, of yielding accurate results.

The crossover point $p \approx b$ is near $(\sin\theta)/\lambda = 0.34$ for Gd at 96 °K. Since we expect the conduction electrons to manifest themselves in the form factor at small scattering angles we have tried to evaluate accurately all corrections for the low-angle reflections. These will be described in a section to follow.

Additionally, since the unpolarized-beam method is capable of high accuracy for just these low-angle peaks, we have used it for evaluation of the magnetic-scattering amplitudes of reflections $(hk0)$ and $(0kl)$ to $\sin\theta/\lambda = 0.517$. Several corrections must be applied to the unpolarized-beam data to obtain precise values of the magnetic-scattering amplitude. These are discussed briefly below.

C. Unpolarized Beam

The integrated intensity in a Bragg reflection (hkl) from an extinction-free ferromagnetic crystal is given by

$$I_{hkl} = KA_{hkl} |G|^2_{hkl} (b^2 + \langle q^2 \rangle p^2) e^{-2B(\sin^2\theta)/\lambda^2} / \sin 2\theta, \tag{2}$$

where K is a scale factor which contains the incident intensity I_0, A_{hkl} is an absorption correction, $|G|_{hkl}$ is the known geometrical structure factor for the reflection (hkl), p and b are as in Eq. (1) above, q is a quantity which depends on the angles the magnetic moments make with the scattering vector, and must be averaged over the domain distribution, and B is the Debye-Waller temperature factor.[14] Our experiment consists of measuring the integrated intensity of a series of Bragg reflections at a low temperature where the magnetic reflections

are well developed, and again at a temperature above the Curie point, and in zero applied field, where the nuclear scattering only appears in the Bragg reflections. To eliminate the domain population as an unknown parameter the low-temperature measurements were carried out in a vertical external field of 12.5 kOe, a field sufficiently strong to align all moments in the vertical direction and hence to make $\langle q\rangle^2 = 1$ for all reflections. Under the conditions cited the integrated intensities at the low and high temperature become

$$I^L_{hkl} = K^L A^L_{hkl} |G|^2_{hkl} (b^2 + p^2) \exp[-2B^L(\sin^2\theta^L)/\lambda^2]/\sin 2\theta^L,$$
$$I^H_{hkl} = K^H A^H_{hkl} |G|^2_{hkl} b^2 \exp[-2B^H(\sin^2\theta^H)/\lambda^2]/\sin 2\theta^H, \quad (3)$$

where the symbols L and H refer to quantities characteristic of the low and high temperature, respectively. The ratio of intensities at the two temperatures, corrected for changes in scale factor, absorption, Debye-Waller factor, and Bragg angle with temperature, yields the value of p/b at the lower temperature. Measurements were made on crystals 1 and 2 at neutron wavelengths of 1.07, 0.77, and 0.65 Å at 96 °K, the same temperature at which the polarized-beam measurements were made, and at 309 °K.

The Debye-Waller factor ratio was measured directly in a separate experiment. The specimen was placed in a horizontal field at 96 °K with which the magnetic contributions to the (002), (004), and (006) reflections could be extinguished, and the resultant nuclear intensities were compared with those measured at 309 °K in zero field. In this experiment, as well as in the primary one, care was taken to measure the change in the incident intensity, and hence in K, due to inhomogeneity of the incident beam. (With thermal contraction of the system on cooling the crystal was in a different part of the beam at the two temperatures.)

Small calculated corrections were applied to the intensity ratios to take into account thermal expansion of the specimens (change in Bragg angle) and changes in thermal and paramagnetic scattering (change in effective absorption).

Finally, it was observed that the very low-angle reflections at 1.07 Å appeared to be influenced by extinction. Accordingly these data were excluded from the final compilation. In the case of crystal No. 2 the questionable reflections were measured at a third wavelength of 0.65 Å. In every case small extinction corrections based on the observed mosaic widths of the crystals were applied to the data.

The results of these experiments will be presented and discussed, following a description of the polarized-beam measurements to which we now turn.

D. Polarized Beam

Equation (1), which relates p/b to the flipping ratio R, must, in a real experiment, be modified to take account of imperfections in the operation of the instrument and of certain perturbing characteristics of the sample. We describe these modifications briefly here and give a more detailed treatment of the general problem (diffraction of polarized neutrons by a specimen with extinction, spin-flip scattering, and depolarization) in the Appendix. This treatment is an extension of one given by Moon[15] in his study of hexagonal cobalt.

We show in Table II some typical values of these corrections for reflections for which $p/b > 1$, $p/b \cong 1$, and $p/b < 1$. It may be noted that data taken under widely different experimental conditions are in good agreement after the corrections are made.

a. Instrumental imperfections. The data are subject to correction for imperfect incident polarization, imperfect spin reversal, and half-wavelength contamination. As shown in the Appendix, the first two corrections can be assessed by means of a double analyzer. Typically, values of $P_0 = 0.992 \pm 0.004$, $P_f = 0.996 \pm 0.004$, and $P_a = 0.994 \pm 0.001$ were evaluated where P_0, P_f, and P_a refer, respectively, to the efficiencies of the polarizer, flipper, and analyzer.[16] The influence of these imperfections on the values of p/b is shown in Table II columns headed $\Delta(\delta_0 + \delta_f)$ and $\Delta(\delta_f)$. The half-wavelength correction is given under Δ_h.

b. Depolarization. By far the most troublesome sample property with which we had to deal was the depolarization of the incident beam. It is possible to measure the depolarization of the beam on transmission through the sample, but unless the source of the depolarization is known, its effect on the Bragg reflections is difficult to assess accurately. We have assumed a uniform-volume depolarization in order to make the necessary corrections, although our treatment would also apply if the depolarization were a surface effect occurring equally at the entrance and exit surfaces. On this model a combination of the flipping ratio of the straight-through beam with and without the sample in place yields a value for a linear depolarization coefficient with which the Bragg reflection data can be corrected. The uncertainties in this correction are most important in the vicinity of $p/b = 1$; it is in just the range of scattering vectors for which this is the case, however, that an assessment of the validity of the depolarization correction can be made. One may, by varying the temperature, adjust the value of p for such a reflection so that the observed flipping ratio goes through a maximum. At this maximum value there is no extinction correction and $1/R_{max} = \delta_0 + \delta_f + \delta_D$, where δ_0, δ_f, and δ_D represent departures from perfection in the in-

TABLE II. Representative corrections to polarized-beam p/b values. The column headed by p/b (raw) was calculated from Eq. (A28) by setting $P_x = P_x'$. The other columns were calculated as described in the Appendix. The final value is not always equal to the sum of p/b (raw) plus all corrections because of the nonlinear nature of p/b as a function of P_x.

Crystal	λ (Å)	p/b (raw)	$\Delta(\delta_0+\delta_f)$	$\Delta(\delta_f)$	$\Delta(\mu_d)$	Δ_h	Δ_{EX}	$\Delta(\gamma^{+-})$	p/b (final)
	Reflection (010)		$(\sin\theta)/\lambda = 0.1592$		$(p/b)_{av} = 1.731 \pm 0.006$			No. of det. = 13	
1	1.07	1.824	−0.0183	0.0007	−0.0483	−0.0021	−0.0205	0.0001	1.736 ± 0.015
1	0.85	1.836	−0.0392	0.0016	−0.0372	−0.0015	−0.0162	0.0	1.743 ± 0.017
1	0.77	1.813	−0.0305	0.0012	−0.0272	−0.0010	−0.0128	0.0	1.743 ± 0.013
2	1.07	1.942	−0.0614	0.0029	−0.0692	−0.0020	−0.0671	0.0012	1.748 ± 0.025
2	0.77	1.827	−0.0291	0.0012	−0.0679	−0.0010	−0.0237	0.0001	1.707 ± 0.016
	Reflection (022)		$(\sin\theta)/\lambda = 0.3622$		$(p/b)_{av} = 0.929 \pm 0.017$			No. of det. = 7	
2	1.07	0.775	0.0197	−0.0002	0.0791	0.0020	0.0020	0.0	0.902 ± 0.033
2	0.77	0.741	0.0810	−0.0009	0.0434	0.0007	0.0015	−0.0001	0.912 ± 0.052
2	0.77	0.781	0.0310	−0.0002	0.0832	0.0009	0.0010	0.0	0.940 ± 0.044
	Reflection (040)		$(\sin\theta)/\lambda = 0.6369$		$(p/b)_{av} = 0.2548 \pm 0.0011$			No. of det. = 4	
1	1.07	0.2465	0.0022	−0.0003	0.0039	0.0003	0.0005	0.0	0.2531 ± 0.0030
1	0.77	0.2498	0.0026	−0.0003	0.0023	0.0001	0.0002	0.0	0.2547 ± 0.0018
2	1.07	0.2433	0.0051	−0.0007	0.0057	0.0003	0.0011	0.0	0.2548 ± 0.0019

cident-beam polarization, flipping efficiency, and depolarization. From separate experiments $\delta_0 + \delta_f$ is known, and thus the depolarization coefficient can be established. In all cases studied the two methods gave approximately the same results. Consequently we have some confidence that we have adequately handled the depolarization problem. Corrections to p/b due to depolarization are given under $\Delta(\mu_d)$ in Table II.

Inspection of Eq. (1) shows that p/b is a double-valued function of the flipping ratio, and it is not always obvious which choice to make. This is particularly true near $p/b = 1$. The same experiments in which the temperature was varied to establish a depolarization correction also served to remove this ambiguity. If $p/b < 1$, the flipping ratio will increase when the temperature is decreased, while the opposite is true for $p/b > 1$.

c. Sample misalignment. The two samples on which most of the experiments were done were not perfectly oriented in the sense that the figure axes were not exactly parallel to the c and a directions, respectively. In the course of the experiments it was sometimes necessary to tilt the magnet (and the sample) about the horizontal rotation axis in order to put the scattering vector into the plane of the counter. In most cases the angle of tilt required was 2° or 3°, but for a few reflections angles as great as 8° were necessary. The magnetization, therefore, was not always normal to the scattering vector, and this results in a number of troublesome but not serious corrections.

The major effect of the misalignment is that the magnitude of the magnetic-interaction vector $\vec{q}$ is not exactly unity. The scattering cross sections are functions of q, but they are readily calculated and this effect has been included in the raw p/b values listed in Table II. A secondary effect is that the spin-flip scattering is nonzero for $q \neq 1$. This modifies the extinction correction slightly. The correction for spin-flip scattering is listed in Table II as $\Delta(\gamma^{+-})$.

d. Extinction. As in the case of the unpolarized-beam experiments, measurements were made under conditions for which secondary extinction was expected to be small, and the importance of extinction was judged from measurements made at several wavelengths. Calculated corrections based on the measured mosaic spread parameters were applied. The conventional expressions were modified slightly because of the misalignment of the sample. These corrections appear in Table II under Δ_{EX}.

e. Simultaneous reflections. As shown by Moon and Shull[17] these effects will be small for pillar-shaped crystals with low extinction. While we have not performed azimuthal scans to search for simultaneous reflections, the reproducibility of our results for different wavelengths, different but equivalent reflections, and different crystals, gives us confidence that the data are largely free of errors from this source.

f. Magnetic anisotropy and depolarization. Although the magnetic anisotropy of gadolinium is small compared to the other heavy rare earths, it is nevertheless not negligible. At 96 °K the easy direction of magnetization makes an angle of approximately 45° with the c axis. In the applied field of 12.5 kOe, and with the pillar-shaped specimens, the magnetization is rigorously parallel to the field direction only for fields directed along the c axis, in the basal plane, or at 45° to the c axis. For other directions the beam polarization and the

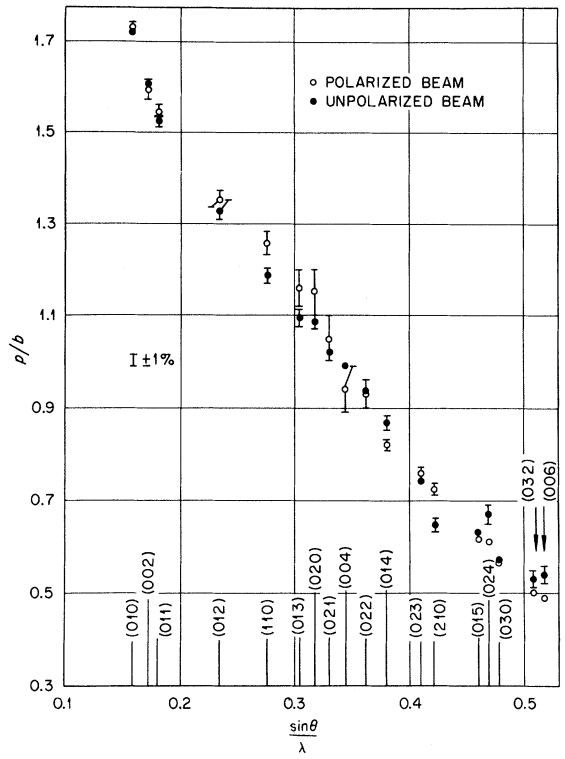

FIG. 1. Comparison of polarized- and unpolarized-beam data for the small-angle region in ^{160}Gd. Error bars represent the result of statistical analysis of individual determinations and a best estimate of possible systematic errors. The agreement of the two sets of data for reflections for which $p \approx b$ indicates that corrections to the polarized-beam data have been adequately handled.

magnetic-interaction vector $\vec{q}$ become complicated functions of the direction of the application of the field, and corrections similar to those discussed above under sample misalignment would have to be made. In fact, since the samples were not perfectly oriented, the magnetization was not strictly parallel to the field direction but the departures were very small, and the effects were included in the sample-misalignment corrections as an error in the setting of the magnet.

III. RESULTS

A. Comparison of Polarized- and Unpolarized-Beam Data

Results of the unpolarized-beam experiments, expressed as values of p/b, are shown in Fig. 1 by the filled circles. Polarized-beam data for the same reflections are represented by open points. The two sets of 18 ratios given are averages of measurements made of equivalent reflections with different crystals at different wavelengths. The data presented in Fig. 1 represent 146 individual determinations with the polarized beam, and 86 sets of measurements with the unpolarized beam. The error bars shown have been calculated from a statistical analysis of the errors in the individual determinations, and from estimated errors in the several corrections to the data.

The results of the two types of measurements are generally in good agreement and it is signficant that they pass smoothly through the crossover region. This implies that the polarized-beam data in this region of $(\sin\theta)/\lambda$ have been properly corrected.

B. High-Temperature Polarized-Beam Measurements

Implicit in our data-reduction procedures is the assumption that the Debye-Waller factors for nuclear and magnetic scattering are equal. Although this is a reasonable assumption, we have tried to test it directly by higher-temperature measurements. It was of interest as well to study the temperature dependence, if any, of the form factor.

Measurements of the flipping ratios of reflections $(hk0)$ to $(\sin\theta)/\lambda = 0.84$ and reflections $(0kl)$ to $(\sin\theta)/\lambda = 0.76$ were made at 313 °K in an applied field of 15.5 kOe, under which conditions an average atomic moment of $1.32\mu_B$ was induced. The magnetic-scattering amplitudes were thus very much smaller than those measured at 96 °K and the corrections applied to the observed data, including that for depolarization, were very much less important than for those over the same values of $(\sin\theta)/\lambda$ at the lower temperature.

The results of these measurements as shown in Fig. 2 are presented as ratios of the magnetic-scattering amplitudes at the two temperatures. In each case, within experimental error, the ratio is constant and equal to the ratio of the saturation magnetization at 96° to the induced magnetization at 313 °K. That the constant ratios for the two sets of reflections differ slightly may be due to slightly different magnetic fields, or to slightly different equilibrium temperatures achieved in the two experiments. The discrepancy in any case amounts to a maximum of 2.7%.

These results have three important implications. If it be assumed that the form factor is temperature dependent, and that the Debye-Waller factors for magnetic and nuclear scattering, B_e and B_n, are different, the ratio of magnetic-scattering amplitudes will have the form

$$\frac{p_L}{p_H} = \frac{\mu_L}{\mu_H} \exp\left(+ (B_n^L - B_n^H)\frac{\sin^2\theta}{\lambda^2}\right) \exp\left(- (B_e^L - B_e^H)\frac{\sin^2\theta}{\lambda^2}\right), \tag{4}$$

where the symbols L and H designate the low- and high-temperature value, respectively, of the quantities to which they are attached.

The first exponential term is the nuclear-temperature-factor ratio which, as indicated in an

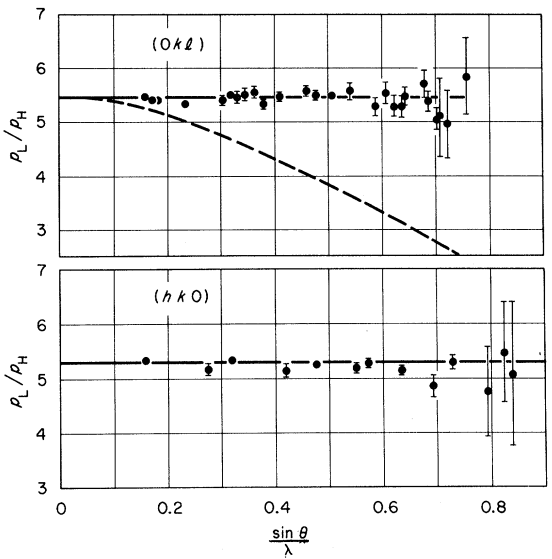

FIG. 2. Comparison of magnetic-scattering amplitudes measured at a high and a low temperature. The lower part of the figure shows that the ratio of p_L/p_H for the ($hk0$) reflections is constant, within experimental errors for all values of $(\sin\theta)/\lambda$. In the upper part of the figure the ratio is shown to be constant for ($0kl$) reflections. That the two constants differ slightly is due, probably, to a small temperature or field difference in the two measurements. The curve shown is the variation of the nuclear Debye-Waller temperature-factor ratio. As explained in the text, this must be compensated for by temperature variation of the electronic Debye-Waller–factor ratio or by a temperature variation of the form factor or both. It is concluded that the form factor is independent of temperature, and that the nuclear and electronic Debye-Waller factors are equal.

earlier section, was measured directly. This function, multiplied by the moment ratio, is shown as the dotted curve in the upper part of Fig. 2. In order to generate the experimental result that $p_L/p_H = \mu_L/\mu_H$ for all reflections, the product $(f_L/f_H) \times\{\exp[-(B_e^L - B_e^H)(\sin^2\theta)/\lambda^2]\}$ must be equal to the inverse of the nuclear-temperature-factor ratio.

If the mean-square amplitude for the electronic displacement is significantly different than that for nuclear displacement, the form-factor ratio would have to depart substantially from unity at large scattering angles in order to fit the experiment.

This is contrary, however, to our expectation that the localized $4f$ form factor would remain unchanged; any changes in spin density we would anticipate to occur in the conduction-electron contribution, since the $4f$ band in metallic Gd is well below the Fermi surface.[18] Accordingly we conclude that (i) the nuclear and electronic Debye-Waller factors are equal, and (ii) the form factor of gadolinium is the same at 96 °K as it is at 313 °K. Conversely, if these conclusions be accepted, the experimental results indicate that the correction procedures used in treating the low-temperature polarized-beam data are correct.

Our observations are consistent with the reasonable assumption that the conduction-electron polarization is proportional to the average z component of the localized $4f$ spin, even above the Curie point when an external field is used to induce a net moment. This is in apparent contradiction with the high-temperature susceptibility data[1] which indicate Curie-Weiss behavior with an effective moment equal to that expected for an $S=\frac{7}{2}$ ion. However, it should be noted that our high temperature of 313 °K is still well below the region of Curie-Weiss behavior of the susceptibility. At this temperature there are strong short-range order correlations, so the sample is not in a real paramagnetic state. It will be interesting to repeat our measurements at significantly higher temperature.

C. Measurement of b for ^{160}Gd

In order to convert the measured p/b ratios to magnetic-scattering amplitudes it is necessary to measure the nuclear-scattering amplitude independently. For that purpose neutron-diffraction studies of the highly enriched oxide Gd_2O_3 were carried out at room temperature.

Gd_2O_3 crystallizes in the bixbyite structure in which there are two sets of nonequivalent metal atom positions, one of which involves a single parameter u. The oxygen ions are in general positions of the space group $Ia3$-T_h^7, and three positional parameters are required. One of the strong low-angle reflections, (222), is independent of the oxygen parameters and insensitive to the exact value of the metal positional parameter.

The intensity of this reflection was measured once in a polarization-analysis experiment and twice with an unpolarized beam from which the scattering amplitude of ^{160}Gd was obtained by comparison with silicon as a standard scatterer. More complete patterns were obtained with the polarized beam (in the course of experiments to be described below designed to measure the paramagnetic-scattering cross section of Gd^{+3}) and with an unpolarized beam. These data were calibrated internally against the scattering amplitude of oxygen. The final result for the scattering amplitude of ^{160}Gd was $b=(0.915\pm0.005)\times10^{-12}$ cm. This is within experimental error of the value $b=0.91\pm0.04$ obtained in an earlier experiment on material of lower isotopic purity[19] (98.7% ^{160}Gd). From a least-squares fitting of the more complete diffraction data the following values for the parameters were evaluated: $u=-0.0304\pm0.0007$, $x=0.3913\pm0.0013$, $y=0.1512\pm0.0012$, $z=0.3811\pm0.0015$. These parameters are close to those obtained in diffraction experiments on other rare-earth ox-

TABLE III. Observed values of p/b and μf for ^{160}Gd.

$h\ k\ l$	$(\sin\theta)/\lambda$	p/b	Error	μf	Error
1 0 1 0	0.1592	1.7250	0.0060	5.854	0.0203
2 0 0 2	0.1725	1.6020	0.0100	5.437	0.0339
3 0 1 1	0.1811	1.5300	0.0110	5.193	0.0373
4 0 1 2	0.2348	1.3390	0.0140	4.544	0.0475
5 1 1 0	0.2758	1.1990	0.0120	4.069	0.0407
6 0 1 3	0.3038	1.1070	0.0180	3.757	0.0611
7 0 2 0	0.3185	1.0900	0.0100	3.699	0.0339
8 0 2 1	0.3299	1.0240	0.0190	3.475	0.0644
9 0 0 4	0.3450	0.9830	0.0190	3.336	0.0645
10 0 2 2	0.3622	0.9300	0.0170	3.156	0.0577
11 0 1 4	0.3800	0.8320	0.0090	2.824	0.0305
12 0 2 3	0.4103	0.7540	0.0090	2.559	0.0277
13 2 1 0	0.4213	0.7070	0.0150	2.399	0.0509
14 0 1 5	0.4597	0.6190	0.0050	2.101	0.0170
15 0 2 4	0.4695	0.6100	0.0030	2.070	0.0102
16 0 3 0	0.4777	0.5640	0.0030	1.914	0.0102
17 0 3 2	0.5079	0.5030	0.0030	1.707	0.0102
18 0 0 6	0.5175	0.4900	0.0030	1.663	0.0102
19 0 2 5	0.5361	0.4320	0.0016	1.466	0.0054
20 0 1 6	0.5414	0.4142	0.0017	1.406	0.0058
21 2 2 0	0.5516	0.3978	0.0012	1.350	0.0041
22 3 1 0	0.5741	0.3575	0.0020	1.213	0.0068
23 0 3 4	0.5892	0.3277	0.0014	1.112	0.0048
24 0 2 6	0.6076	0.3009	0.0024	1.021	0.0081
25 0 1 7	0.6244	0.2734	0.0011	0.9279	0.0037
26 0 4 0	0.6369	0.2548	0.0012	0.8648	0.0041
27 0 4 1	0.6427	0.2476	0.0028	0.8403	0.0095
28 0 4 2	0.6598	0.2220	0.0015	0.7534	0.0051
29 0 2 7	0.6826	0.1941	0.0007	0.6588	0.0024
30 0 4 3	0.6875	0.1922	0.0015	0.6523	0.0051
31 0 0 8	0.6900	0.1847	0.0021	0.6269	0.0071
32 3 2 0	0.6940	0.1768	0.0045	0.6000	0.0153
33 0 3 6	0.7043	0.1728	0.0010	0.5865	0.0034
34 0 1 8	0.7081	0.1663	0.0014	0.5644	0.0047
35 0 4 4	0.7243	0.1484	0.0014	0.5037	0.0048
36 4 1 0	0.7297	0.1407	0.0008	0.4775	0.0027
37 0 2 8	0.7600	0.1159	0.0011	0.3933	0.0037
38 0 4 5	0.7692	0.1089	0.0010	0.3696	0.0034
39 0 1 9	0.7924	0.0873	0.0014	0.2963	0.0047
40 0 5 0	0.7961	0.0816	0.0014	0.2769	0.0048
41 0 5 1	0.8008	0.0819	0.0025	0.2780	0.0085
42 0 5 2	0.8146	0.0756	0.0027	0.2566	0.0092
43 0 4 6	0.8206	0.0590	0.0031	0.2002	0.0105
44 3 3 0	0.8274	0.0624	0.0012	0.2118	0.0041
45 0 5 3	0.8371	0.0569	0.0019	0.1931	0.0064
46 0 2 9	0.8390	0.0563	0.0023	0.1911	0.0078
47 0 3 8	0.8392	0.0553	0.0019	0.1877	0.0065
48 4 2 0	0.8425	0.0583	0.0020	0.1978	0.0068
49 0 0 10	0.8625	0.0422	0.0028	0.1432	0.0095
50 0 5 4	0.8677	0.0453	0.0030	0.1537	0.0102
51 0 1 10	0.8771	0.0374	0.0024	0.1269	0.0081
52 0 4 7	0.8776	0.0353	0.0022	0.1198	0.0075
53 5 1 0	0.8865	0.0313	0.0011	0.1062	0.0037
54 0 5 5	0.9054	0.0202	0.0030	0.0686	0.0102
55 0 4 8	0.9390	0.0068	0.0029	0.0231	0.0099
56 0 5 6	0.9495	0.0047	0.0037	0.0160	0.0126
57 0 6 0	0.9554	0.0008	0.0011	0.0027	0.0037
58 0 1 11	0.9620	−0.0017	0.0035	−0.0057	0.0114
59 4 3 0	0.9685	−0.0015	0.0016	−0.0051	0.0051
60 0 6 2	0.9708	−0.0023	0.0014	−0.0078	0.0047
61 0 3 10	0.9860	−0.0051	0.0029	−0.0173	0.0098
62 5 2 0	0.9944	−0.0121	0.0005	−0.0411	0.0017
63 0 5 7	0.9992	−0.0087	0.0016	−0.0295	0.0054
64 0 2 11	1.0008	−0.0141	0.0044	−0.0479	0.0149
65 0 0 12	1.0350	−0.0222	0.0019	−0.0753	0.0064
66 6 1 0	1.0441	−0.0188	0.0022	−0.0638	0.0075
67 4 4 0	1.1031	−0.0325	0.0011	−0.1103	0.0037
68 5 3 0	1.1146	−0.0346	0.0022	−0.1174	0.0074
69 0 7 0	1.1146	−0.0270	0.0013	−0.0916	0.0044
70 6 2 0	1.1482	−0.0400	0.0018	−0.1358	0.0061
71 7 1 0	1.2021	−0.0401	0.0010	−0.1361	0.0034
72 5 4 0	1.2436	−0.0425	0.0024	−0.1442	0.0081
73 6 3 0	1.2638	−0.0430	0.0021	−0.1459	0.0071
74 0 8 0	1.2738	−0.0425	0.0041	−0.1442	0.0139

TABLE III (*Continued*)

ides[20–22] and differ only slightly from those derived from data on bixbyite itself.[23]

D. Summary of Measurements

The corrected values of p/b measured at 96 °K for all $(hk0)$ reflections to $(\sin\theta)/\lambda = 1.275$ and for nearly all $(0kl)$ reflections to $(\sin\theta)/\lambda = 1.04$ are summarized in Table III. (For subsequent Fourier syntheses, interpolated values for the several unmeasured reflections were used.) In general, each entry represents an average over equivalent reflections of measurements on different crystals at different neutron wavelengths. In the low-angle region the data shown are weighted averages of the results of the unpolarized- and polarized-beam data. In all, 350 distinct flipping-ratio measurements were made. As indicated above, 172 distinct integrated intensities were measured in the unpolarized-beam experiments.

The errors indicated in the table are based on a statistical analysis of the individual measurements, and on estimated errors in the corrections applied. The procedure is indicated in the Appendix. Also shown in the table are values of the product μf obtained from the p/b ratios with the experimentally determined value for the nuclear-scattering amplitude of ^{160}Gd.

In Fig. 3 the results of the measurements are compared with a theoretical curve based on the Blume-Freeman-Watson form factor.[24] This curve is normalized to a $4f$ moment of $6.42\mu_B$. At the experimental temperature of 96 °K and applied field of 12.5 kOe the total magnetic moment is $6.92\mu_B$.[1] On the assumption that the $4f$ contribution has the same temperature dependence as the total moment, a value of $6.42\mu_B$ for the $4f$ moment is expected.

Several points are immediately obvious from this figure. It is clear that the experimental data fall consistently below the calculated curve, except for the first two points, and thus that the free-ion wave functions of Freeman and Watson[25] are more contracted than actual $4f$ wave functions in the metal.[26] Inspection of the data, particularly at the higher angles where there is a high density of reflections, shows that they fall smoothly with increasing scattering angle. This implies that the spin distribution is spherically symmetric, as might

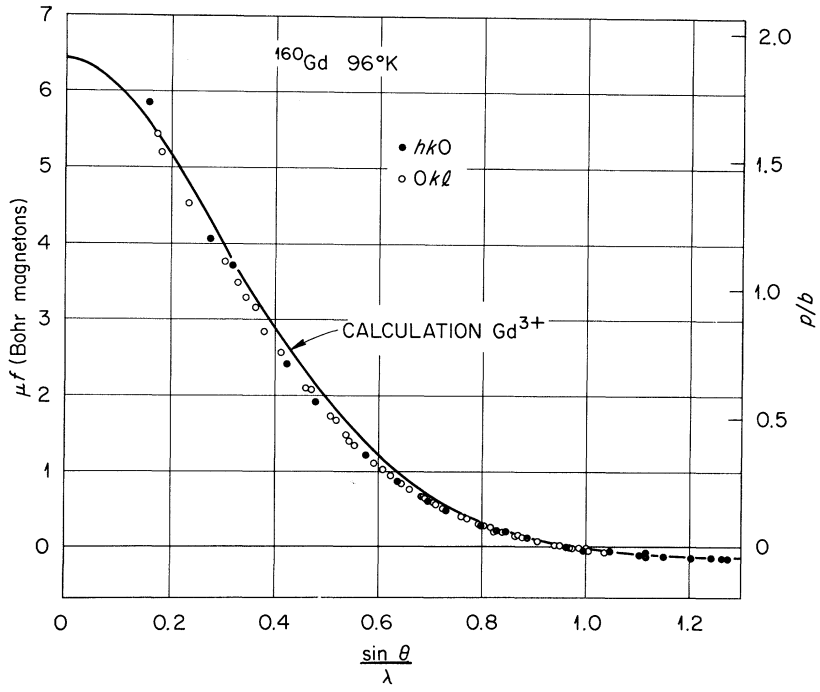

FIG. 3. Magnetic-scattering amplitudes of ^{160}Gd at 96 °K. The weighted-average values of p/b, right-hand scale, and of μf, left-hand scale, for all observations are shown by open or closed circles. The size of the circle is a measure of its error. The line is the calculation of the Gd^{+3} form factor due to Blume, Freeman, and Watson, normalized to $6.42\mu_B$, the expected $4f$ moment at 96 °K and in 12.5 kOe.

be expected from S-state ions. As we shall see presently, it is possible from a Fourier synthesis to state that the $4f$ spin density departs from spherical symmetry by less than 1%. There is an abrupt change in slope of the experimental data near $(\sin\theta)/\lambda = 0.18$. This, we believe, is associated with conduction-electron polarization.

We consider the further analysis of these data and its implications with regard to the points just mentioned in Sec. IV.

IV. ANALYSIS AND CONCLUSIONS

A. Separation of Local and Diffuse Spin Distributions

The data given in Table III can be used to make projections of the moment density or, since we are dealing with an S-state local moment, of the unpaired spin density. It will be instructive to examine first profiles of the projected densities in certain important directions in the crystal.

The projected density on the basal plane is given by

$$\rho(\vec{r}) = A^{-1}\sum_h \sum_k F_{hk0}\, e^{-i\vec{k}_{hk0}\cdot\vec{r}}\,. \tag{5}$$

The double sum extends over all reciprocal-lattice vectors in the basal plane, and A is the area of the unit-cell projection. The structure amplitude is

$$F_{hk0} = \sum_j (\mu f)_{hk0}\, e^{i\vec{k}_{hk0}\cdot\vec{r}_j}, \tag{6}$$

where the sum is over the position vectors of atoms in the unit cell, and μ is the magnetic moment per atom. A similar expression can be written for the $(0kl)$ data. It is convenient to choose a pseudo-orthorhombic unit cell for the hexagonal close-packed structure the dimensions of which are a, $\sqrt{3}a$, and c. In this cell the atoms are found at $(0, \frac{1}{3}, \frac{3}{4})$; $(0, \frac{2}{3}, \frac{1}{4})$; $(\frac{1}{2}, \frac{1}{6}, \frac{1}{4})$; and $(\frac{1}{2}, \frac{5}{6}, \frac{3}{4})$.

In the upper part of Fig. 4, the projected density on the basal plane is shown as a function of distance from an atomic site along the line shown in the insert. The solid line is the experimental total point density. The resolution function is calculated with a constant form factor for each reflection and scaled to the total point density at $r = 0$.

On an expanded scale in the center of the figure is shown the projected density away from the atomic sites. To avoid complications from series-termination effects, and since the density in this region is slowly varying, we have calculated a spherical average density following the procedure given by Moon.[27] The radius of the averaging sphere is 0.63 Å. It will be noted that this average density goes negative in the region between the projected atomic sites. The midpoint, at 2.1 Å, corresponds to the projection of a vacant C site in the usual designation of stacking of A-, B-, and C-type layers in forming close-packed structures. For comparison we have calculated the corresponding profiles for the localized $4f$ moment with the Watson-Freeman-Blume form factor. Comparison of the experimental and theoretical curves shows again that the theoretical wave functions do not adequately describe the spin distribution around the atomic sites; away from the atoms, the calcu-

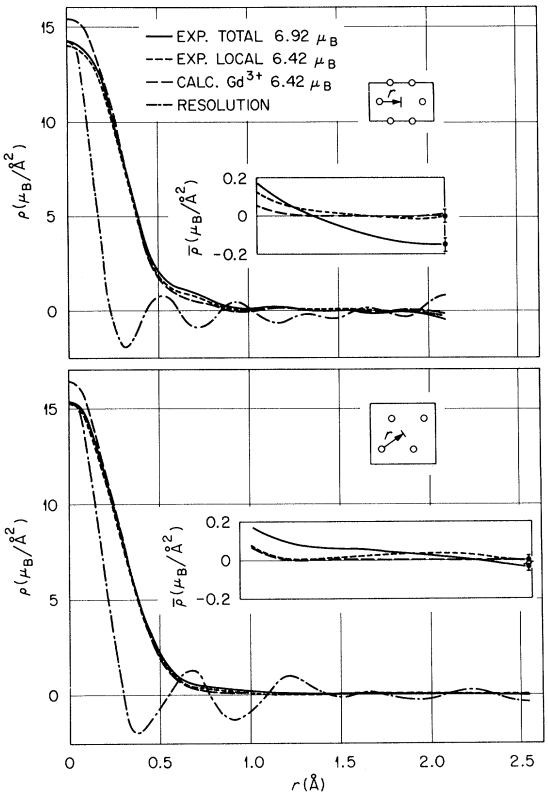

FIG. 4. Projected-moment densities. In the upper part of the figure the total moment density projected onto the basal plane is shown, by the solid line, as a function of distance from the atomic site. The dotted line represents the corresponding projection of the local-moment density (see text). The dashed line is calculated using the Blume-Freeman-Watson form factor for Gd^{+3} and the same set of ($hk0$) reflections. The resolution function is normalized to the total moment density at $r=0$. In the insert are shown the projections of the spherically averaged total, local, and theoretical densities away from the atomic sites. The radius of the averaging sphere is 0.63 Å. The lower part of the figure displays corresponding projections on the plane normal to a hexagonal a axis. The radius of the averaging sphere is 0.44 Å.

lated $4f$ moment density goes to zero as expected. We shall return to the curve labeled "experimental local" presently.

In the lower half of the figure similar profiles, calculated with the ($0kl$) data, are shown along the line indicated. In between atoms the average density oscillates with small amplitude around zero. The width of the first maximum of the resolution function is somewhat greater in this case, because the ($0kl$) data do not go as far out in $(\sin\theta)/\lambda$ as do the ($hk0$).

The projection profiles shown in Fig. 4 suggest that the unpaired spin density sensed by the neutron consists of a localized $4f$ part, and a diffuse part, most probably due to unpaired conduction-electron density. As we have shown earlier,[11] the separation of these two contributions may be made in a logical manner. We repeat the argument here briefly for completeness.

The total moment density $\rho_T(\vec{r})$ is considered to consist of two parts $\rho_L(\vec{r})$ and $\rho_D(\vec{r})$, where ρ_L and ρ_D are the local and diffuse densities so that

$$\rho_T(\vec{r}) = \rho_L(\vec{r}) + \rho_D(\vec{r}) \ . \tag{7}$$

The three functions are periodic with the periodicity of the lattice; thus each may be represented as a Fourier series

$$\rho_\alpha(\vec{r}) = (1/V)\sum_j F_{\alpha j}\, e^{-i\vec{k}_j\cdot\vec{r}} \ , \tag{8}$$

where V is the volume of the unit cell, α runs over the subscripts T, L, and D, and j over all reciprocal-lattice points. The measurements give the set of coefficients F_{Tj} which in our case correspond to reflections ($hk0$) and ($0kl$). If $\rho_D(\vec{r})$ is a slowly varying function of $\vec{r}$ only the first few terms in the Fourier series describing this function will be nonzero.

Inspection of Fig. 5, in which are plotted the first few Fourier coefficients, suggests that only the first three reflections and the zero intercept (the total moment) are affected by ρ_D.

On the assumption that $F_{Dj}=0$ for $(\sin\theta)/\lambda \geq 0.235$, $F_{Tj}=F_{Lj}$ over this range of $(\sin\theta)/\lambda$. Then we require of $\rho_L(\vec{r})$ that it be sufficiently localized that it go to zero between neighboring sites, and we adjust the scattering amplitudes for the first three reflections so that, when combined with the rest of the data in a Fourier series, a constant value of $\rho_L(\vec{r})$ is obtained in the region between atoms. This constant value should be zero if the (000) structure factor is based on $6.42\mu_B$/atom and if $\rho_L(\vec{r})$ describes the $4f$ electrons.

For the basal-plane projection, the $(010)_{hex}$ amplitude is the only adjustable parameter, and, as we have shown before, excellent local-moment behavior is obtained if the (010) amplitude is reduced to fall on the linearly extrapolated portion of the curve of Fig. 5. Thus with the observed value of $(\mu f)_{010}=5.854$ the spherically averaged spin density in the basal-plane projection is as shown in the solid line in the top part of Fig. 4. With $(\mu f)_{010}=5.400$, the "local" value, the dashed curve labeled "Exp. local" is obtained and it is zero, within experimental error, over a fairly large area near the midpoint of the two atoms. Similar results have been obtained with the ($0kl$) data by reducing the (002) and (011) amplitudes to the linear extrapolation of Fig. 4.

The contribution of the diffuse component to the scattering amplitude is given by the difference between the experimental results and those describing the local component. This difference, about which we shall have more to say presently, is shown in

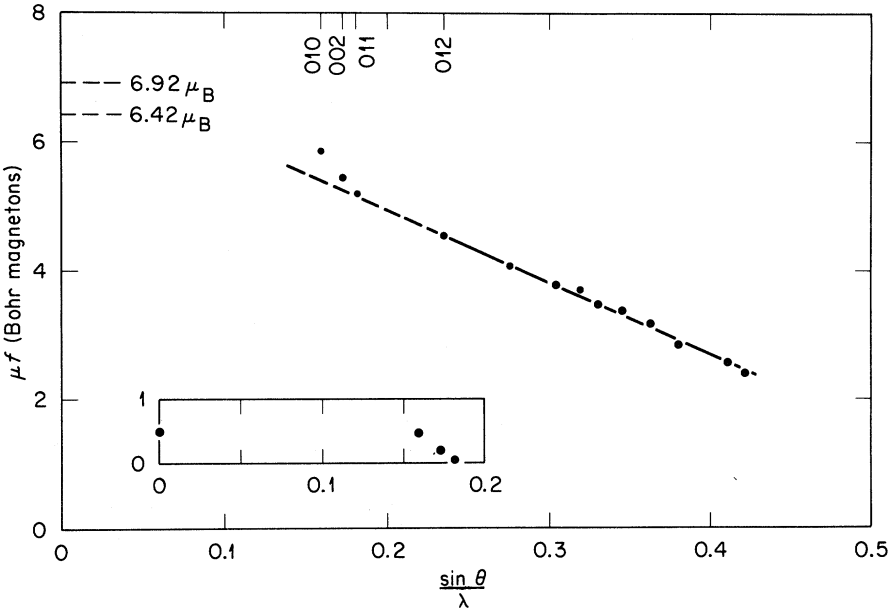

FIG. 5. Magnetic-scattering amplitudes for low-angle reflections in ^{160}Gd. Experimental errors are indicated by the size of the data-point circles. The insert shows scattering amplitudes for the diffuse contribution.

the insert to Fig. 5.

We believe that the local form factor describes the 4*f* electrons for a number of reasons. Most convincing is the result of the local-moment calculation[27] which gives the integral of moment density above the flat region between atoms as $(6.44 \pm 0.16)\ \mu_B$, in excellent agreement with the expected value of $6.42\ \mu_B$ for the 4*f* electrons. The change in the local-moment calculation when $(\mu f)_{010}$ is changed from the observed value to the "local" value is shown in Fig. 6. The dashed line indicates the expected 4*f* moment.

In addition, appeal may be made to some general properties of calculated ionic 4*f* form factors. For small values of $(\sin\theta)/\lambda$ atomic form factors have the functional form

$$f = 1 - A[(\sin^2\theta)/\lambda^2]\ . \qquad (9)$$

For higher values of $(\sin\theta)/\lambda$ the curvature is positive and there is an intermediate region where the curve is nearly linear. From a knowledge of the slope in the linear region, the zero intercept in the quadratic region, and the condition that the functions and their first derivatives be equal at the boundary, one may calculate the value of $(\sin\theta)/\lambda$ corresponding to this boundary. With the experimental data for Gd, it is found that the linear region of Fig. 5 should extend to $(\sin\theta)/\lambda = 0.143$, which is well inside the first Bragg peak. Thus the local form factor which we have extracted from the observations has behavior consistent with that of theoretical 4*f* form factors in the small-angle region. We therefore take the experimental local form factor as representing the unpaired 4*f* spin distribution in Gd.

A contour map of the basal-plane projection of the spherically averaged total density is shown in the upper part of Fig. 7; the corresponding spherically averaged local density is shown in the bottom part of the figure. The density around each atomic site is circular and the diffuse density between sites is negative within the shaded contours. When the value of $(\mu f)_{010}$ is dropped to its "local

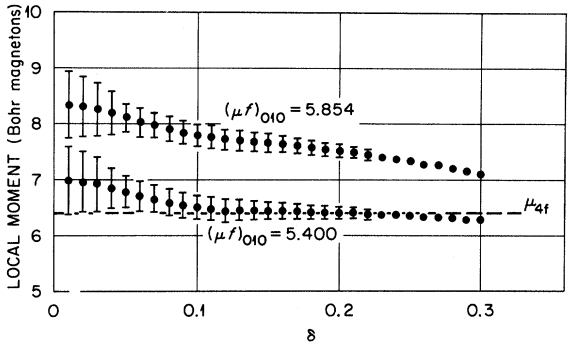

FIG. 6. Change in the local-moment calculation when $(\mu f)_{010}$ is changed to the local value. The calculation is based on a basal-plane projection, along the line $(\frac{1}{2}, \frac{1}{2}, z)$, of the spherically averaged density. The radius of the averaging sphere, in angstroms, is 6.3δ. Below $\delta = 0.06$, the errors bars are an estimate of series-termination errors. Above this value of δ the series-termination errors are smaller than the experimental errors and the error bars indicate the experimental standard deviation. The points shown are an average of the values of the local-moment summation as new terms are added beyond $(\sin\theta)/\lambda = 1.04\ \text{Å}^{-1}$. See Ref. 27 for details. The dashed line indicates the expected 4*f* moment based on the magnetization measurement.

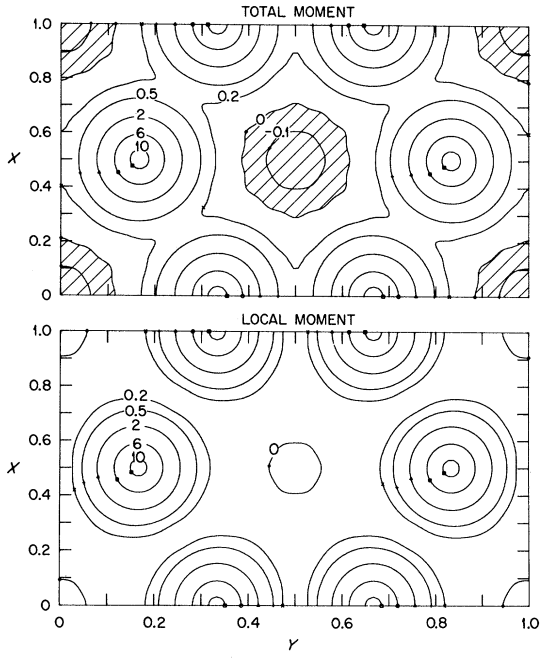

FIG. 7. Contour maps of spherically averaged projected total and local-moment density. The projection is on the basal plane, and the radius of the averaging sphere is 0.63 Å. The numbers on the contour lines are in units of $\mu_B/\text{Å}^2$. Between atomic sites in the total moment projection the moment density goes negative; in the local-moment projection it is zero within experimental error over a considerable distance.

value," the density map in the lower part of the figure results. The first few contours about each site are circular and the density farthest from every atom in the projection is zero, within the experimental error.

Departures from spherical symmetry would be expected to appear as a difference in density along the c axis and in the basal plane. A projection of the local point density based on $(0kl)$ data is shown in Fig. 8. This projection shows that the $4f$ distribution about the atomic sites is spherical in the sense that the semiaxes of the contours parallel to the c axis and normal to c are equal, to within about 1%.

Consider next the diffuse component of the experimental scattering amplitude which is shown in the insert of Fig. 5. The coefficients of all terms in the series for $\rho_D(\vec{r})$ are zero except for the first three terms and for the zero intercept. By definition this constitutes a complete set of data and the point density of the diffuse component can be calculated throughout the unit cell. Contour maps giving the diffuse magnetization in several principal planes are shown in Fig. 9. At each atomic site there is a maximum density of magnitude $(0.056 \pm 0.012)\mu_B/\text{Å}^3$ (6.6 kg) parallel to the local moment. On moving away from the atomic sites the polarization reverses, reaching a maximum of $(-0.037 \pm 0.004)\mu_B/\text{Å}^3$ (−4.4 kg). Negative polarization is found in slowly undulating columns parallel to the c axis, which run through the C sites of the hexagonal close-packed sequence of layers. An attempt to represent this in a three-dimensional diagram is shown in Fig. 10. The surfaces shown are the zero-level contours of the diffuse distribution. Inside the figures so defined is found the negative polarization.

B. $4f$ Form Factor and $4f$ Spin Density

Having made a reasonable separation of the local and diffuse magnetic-moment densities, we turn now to a consideration of the $4f$ form factor and the $4f$ charge density. The first determinations of rare-earth form factors were carried out with the paramagnetic oxides,[20,28] and the theory, given first by Trammell,[29] utilized screened hydrogenic radial wave functions, in which the screening constant was an adjustable parameter. Subsequently Freeman and Watson[25] generated nonrelativistic Hartree-Fock $4f$ wave functions for the trivalent rare-earth ions, and, with these, Blume, Freeman, and Watson[24] calculated rare-earth form factors. Within the rather large experimental error of the data extant, good agreement with the theory was found.

For ionic gadolinium the theoretical form factor has the simple form

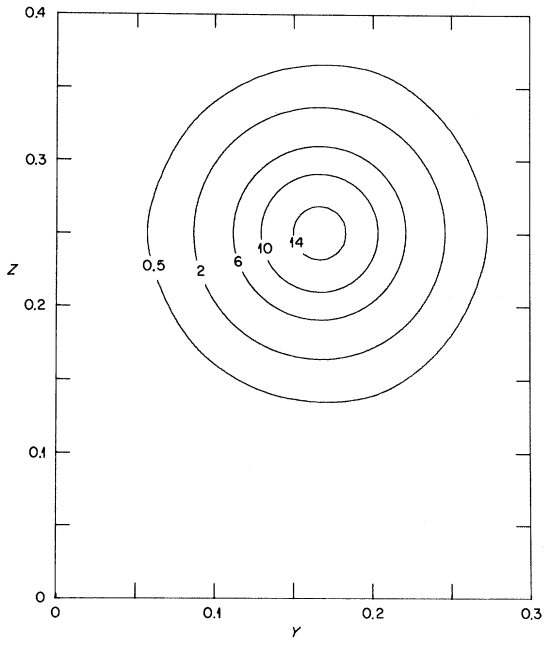

FIG. 8. Contour map of local-moment point density projected on the plane normal to a. The first four contours are circular to within 1%. Numbers on the contour lines are in units of $\mu_B/\text{Å}^2$.

$$f(k) = \langle j_0(k) \rangle = \int_0^\infty U_{4f}^2(r)\, j_0(kr)\, dr\,, \tag{10}$$

where $U_{4f}(r)$ is the Hartree-Fock radial orbital for the $4f$ electron and $j_0(kr)$ is the spherical Bessel function of order zero. The Freeman-Watson wave functions have the convenient analytical form

$$U_{4f}(r) = \sum_{i=1}^{4} C_i r^4 e^{-z_i r}\,, \tag{11}$$

with

$$\int_0^\infty U_{4f}^2(r)\, dr = 1\,. \tag{12}$$

The values of the parameters as given by Freeman and Watson are listed in the first columns of Table IV. The corresponding form factor is, as we have shown in Fig. 1, in poor agreement with our data for the metal.

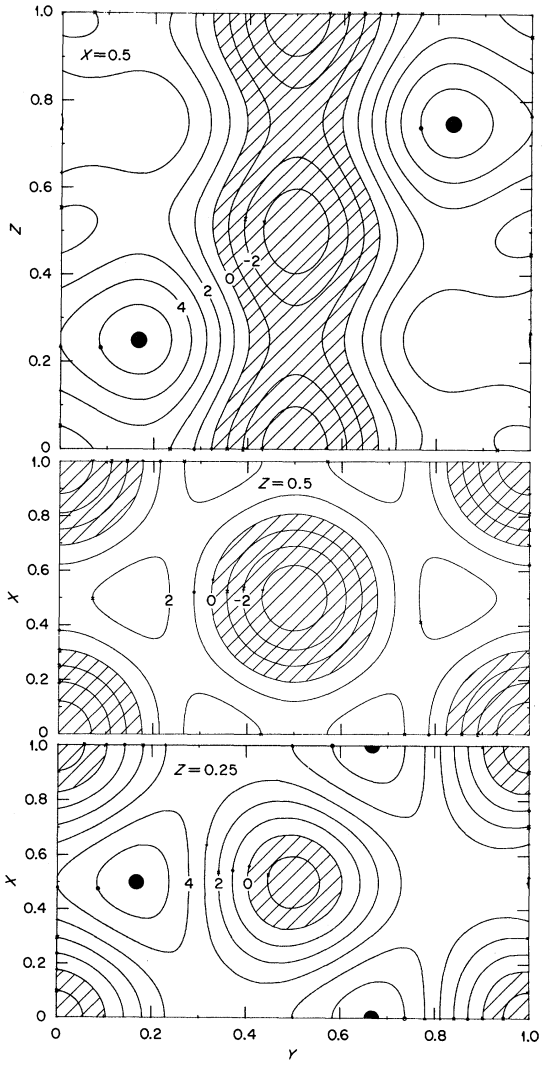

FIG. 9. Contour maps of diffuse component of magnetic-moment density. The shaded areas have negative density values. The numbers on the contour lines are multiples of $0.01\,\mu_B/\text{Å}^3$ or multiples of 1.16 kg. Atomic sites are indicated by black circles. Errors vary from one-half contour interval to about a full interval.

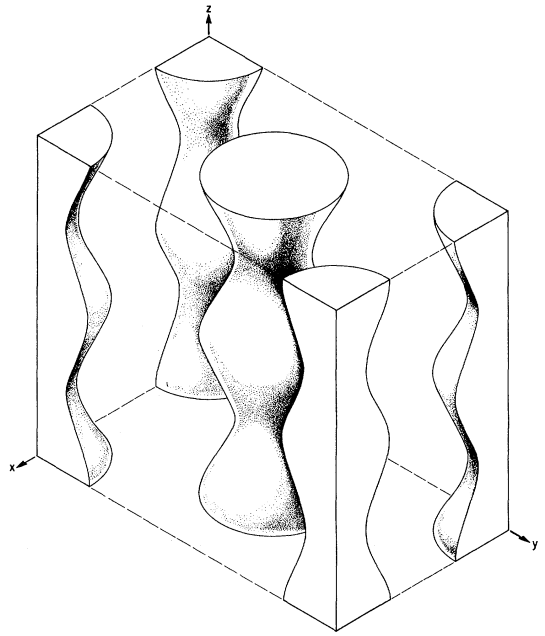

FIG. 10. Distribution of the diffuse component of unpaired spin density in the unit cell. The lines show the zero contour; inside the figures so formed the density is negative.

We have thought it worthwhile to attempt to find an analytical expression for the form factor which would be useful for computational purposes. We have made a least-squares fit of the experimental local form factor to wave functions of the Freeman-Watson type. A similar treatment for Tb and Tm has been described by Brun, Lander, and Felcher.[30] From Eqs. (10) and (11) it can be shown that

$$\langle j_0 \rangle = \sum_{ij} C_i C_j F(z_i + z_j, k)\,, \tag{13}$$

where

$$F(a, k) = 40320\, \frac{a^7 - 7a^5k^2 + 7a^3k^4 - ak^6}{(a^2 + k^2)^8}$$

and k is in inverse atomic units. Our most successful fit was obtained by varying c_1, c_4, z_1, and z_4. The results are shown in Fig. 11 and in the second column of Table IV. The change in c_2 and c_3 from the Watson-Freeman values is a result of renormalizing the form factor obtain in the fitting procedure. It must be emphasized that the wave function which results from this procedure has no fundamental significance but is a convenient analytical representation of our experimental results.

The fit is further illustrated, and on an expanded

TABLE IV. Parameters which define the Hartree-Fock wave functions. The unprimed coefficients define the Watson-Freeman 4*f* orbitals. After least-squares fitting and normalization, the primed coefficients result.

i	Z_i	C_i	Z_i'	C_i'
1	12.554	1923.8151	11.677	1431.8303
2	7.046	329.66724	7.046	297.2024
3	4.697	43.274827	4.697	39.0132
4	2.578	1.5047469	2.602	2.3577

scale, in Fig. 12 for the data obtained at high values of $(\sin\theta)/\lambda$. The smooth behavior of the observations indicates spherical symmetry.

The most obvious reason for the failure of the free-ion Hartree-Fock wave functions to accurately describe the metallic 4*f* electrons is the presence of the conduction electrons in the metallic case. These should provide additional screening of the nuclear charge and allow the 4*f* electrons to move in slightly larger orbits. When the conduction electrons are near the nucleus, they should behave very much as 6*s* or 5*d* electrons in the free atom. Accordingly, Davis and Cooke[31] have undertaken a series of atomic calculations to test the sensitivity of the 4*f* wave functions to the presence of electrons in the 5*d* or 6*s* levels. They used a relativistic Hartree-Fock-Slater program with Wigner-Seitz normalization.[32] In going from the neutral atom ($4f^7\,5d^1\,6s^2$) to the +3 ion ($4f^7$), they found a negligible change in the 4*f* form factor. This is a strong indication that screening by the conduction electrons is not important in determining the radial wave functions in the metal. Davis and Cooke found that their wave functions were quite sensitive to the magnitude of the Slater exchange coefficient, and by varying this coefficient they were able to obtain a 4*f* form factor in rather good agreement with our experimental results. Their calculation for the neutral atom with an exchange coefficient equal to 0.8 times the usual Slater approximation is shown as the dashed line in Fig. 11. It is in excellent agreement with our "local" experimental results at low values of $(\sin\theta)/\lambda$ and is slightly high at larger values of $(\sin\theta)/\lambda$. Because of the arbitrary selection of the exchange parameter, this calculation does not qualify as a theoretical prediction. However, the value of the exchange parameter is reasonable, and the agreement suggests that relativistic effects may be important for the 4*f* wave functions. The excellent agreement with the experimental points in the low-angle region is a further indication that our separation of local and diffuse form factors results in a local form factor of reasonable shape, that is, a shape similar to that expected for the 4*f* electrons.

The radial charge or spin density as calculated by Davis and Cooke is compared with the Watson and Freeman calculation in Fig. 13. The corresponding curve for our least-squares-fitted wave function is so close to the Davis-Cooke result that it is not shown. The maximum in the density function is only slightly different in the three cases, but the Watson-Freeman charge density is significantly contracted compared to the other two cases.

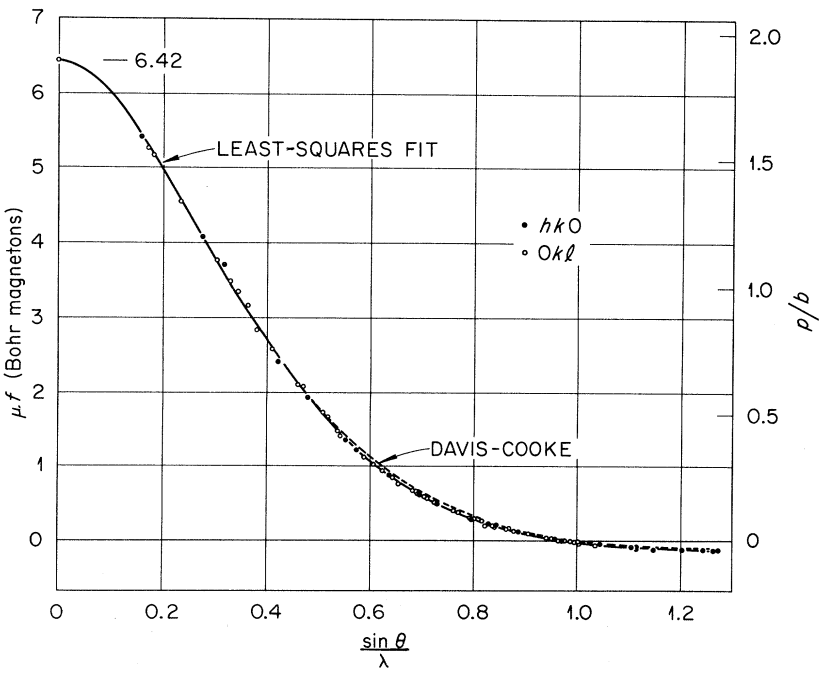

FIG. 11. Comparison of the 4*f* experimental form factor with calculation. The curve labeled Davis-Cooke is based on Hartree-Fock-Slater wave functions. The curve labeled least-squares fit was obtained by varying parameters in the Freeman-Watson 4*f* orbitals.

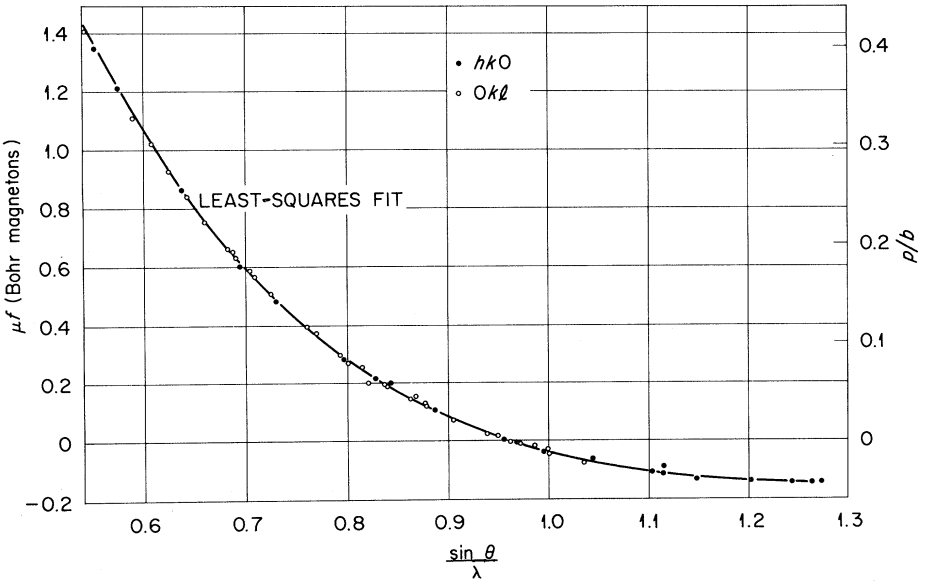

FIG. 12. Comparison at high scattering angles of the experimental data and the least-squares-fit form factor. The data points fall smoothly on the curve.

A measure of the degree of difference between the three density functions is given by calculating $\langle r^2 \rangle$. For the Watson-Freeman function, $\langle r^2 \rangle = 0.785$; for Davis-Cooke, $\langle r^2 \rangle = 0.97$; and for the least-squares fit, $\langle r^2 \rangle = 0.942$.

Another source of unpaired spin density which has thus far been ignored is the core polarization. This is a major contributor to the effective field seen by the nuclei, but has a very small influence on our result. Watson and Freeman[33] have published a radial spin density for the core electrons in Gd^{+3} based on a spin-polarized Hartree-Fock calculation. Unfortunately, the $5p$ contribution was not included. We have obtained a complete set of analytic spin-polarized wave functions for Eu^{+2} from Watson[34] in order to estimate the importance of the core polarization in our results. Based on these wave functions we calculate a form factor which starts at zero, rises to a maximum of 0.05 (in μf units) at $(\sin\theta)/\lambda = 0.2$, and remains small and negative beyond $(\sin\theta)/\lambda = 0.4$. It is typically about 1% of our observed μf values and is comparable to our experimental error. Watson and Freeman[33] have emphasized the negative polarization of the core electrons at large distances. The Eu^{+2} calculation indicates that this outer negative core polarization is a very minor contributor to our diffuse negative density. At a distance of 2.1 Å the core polarization amounts to $-3.3\times10^{-4}\mu_B/\text{Å}^3$, while the maximum in our diffuse density is $-3.7\times10^{-2}\mu_B/\text{Å}^3$. On the basis of the Eu^{+2} calculation, we feel justified in ignoring the core polarization.

Interband mixing has been invoked to account for negative conduction-band polarization in some rare-earth compounds[35] and for a negative g shift in gadolinium.[36] We know there is an interaction between the $4f$ and conduction electrons, and the question of whether this interaction can mix sufficient conduction-electron character into the $4f$ wave functions to significantly alter their shape is very interesting. It seems unlikely that this is the case because the $4f$ band lies at least 6 eV below the Fermi surface.[18]

C. Conduction-Electron Form Factor and Spin Density

Theoretical calculations have not yet reached a stage where realistic conduction-electron form factors exist, so that a comparison of the data shown

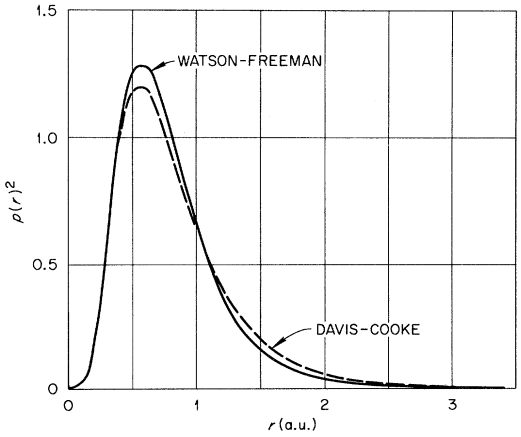

FIG. 13. Radial charge densities calculated from the Freeman-Watson and Davis-Cooke wave functions. The corresponding curve for the least-squares wave functions is indistinguishable from the Davis-Cooke curve on the scale of this figure. Comparison shows the Freeman-Watson wave functions to be more contracted than those in the metal.

in the insert of Fig. 5 or of the unpaired spin density maps with theoretical predictions is not yet possible. The measured diffuse component shown in Fig. 5 is not what is expected for $5d$ or $6s$ electrons in atomic Gd, nor does it correspond to the spin polarization produced in a free-electron gas by the Ruderman-Kittel-Kasuya-Yosida (RKKY) interaction. However, the diffuse component is definitely long range and oscillatory, and these are properties which are universally attributed to conduction electrons in the rare-earth metals.

D. Ionic Form Factor

The paramagnetic-scattering cross section for Gd^{+3} in Gd_2O_3 has been measured[19] with a sample of 98.7% isotopic enrichment. Since a contaminant of just 1% ^{157}Gd is worth 1000 b at 70 meV, the absorption cross section of this specimen was appreciable. Moreover, in the conventional experiment the paramagnetic scattering cross section cannot be measured with high accuracy except at very small scattering angles because of the difficulty in resolving the background from overlapping nuclear reflections superimposed on it.

In the course of this study we have repeated the experiment with a less-absorbing sample, and with the polarization-analysis technique.[37] The experiment is so designed that the polarization of the incident beam is maintained parallel to the scattering vector. A diffraction pattern of the polycrystalline specimen is recorded with the flipper off and with the flipper on. In the former case, only those neutrons which are scattered without spin flip are passed by the polarization-sensitive analyzer and detected by the counter. With the flipper on, only those processes which produce a spin flip on scattering produce detectable neutrons. With the isotopically pure sample (except for small and calculable background effects) the coherent nuclear scattering alone is detected with the flipper off; the paramagnetic scattering alone is detected with the flipper on. A typical set of data is shown in Fig. 14. It is to be noted that useful data for the paramagnetic-scattering cross section are obtained even under the Bragg peaks. A clean separation, therefore, of the magnetic scattering from the nuclear scattering can be achieved. Very small corrections to the spin-flip data were calculated to correct for multiple scattering and instrumental imperfections.

Since the ordering temperature for Gd_2O_3 is below 4.2 °K,[19] we expect the room-temperature paramagnetic scattering to be very closely elastic with no short-range order. The data of Fig. 14 were converted to absolute cross sections by comparison with a silicon-powder pattern. The paramagnetic cross section is given by

$$\frac{d\sigma}{d\Omega} = \frac{2}{3}\left(\frac{\gamma e^2}{mc^2}\right)^2 S(S+1)f^2. \tag{14}$$

We obtained the form factor with no adjustable parameters by taking $S=\frac{7}{2}$.

The oxide form factor is compared with the local metallic form factor in Fig. 15. There is a significant difference between the two experimental form factors, indicating that the oxide spin density is more contracted than the metallic $4f$ density. The oxide form factor is seen to be in good agreement with the Blume-Freeman-Watson calculation except at very small scattering angles.

We have no satisfactory explanation for the difference between the two observed form factors. The most obvious physical difference is the presence of conduction electrons in the metallic case, but the Davis-Cooke calculations tell us that the $4f$ spin density is insensitive to these electrons. Relativistic effects should be equally important in the two cases. We are left with the conclusion that the crystalline environment affects the $4f$ spin density in one or both of these cases in ways that are still to be determined.

V. SUMMARY

The main conclusions of this set of measurements may be summarized as follows:

(i) The total spin density of metallic Gd can be

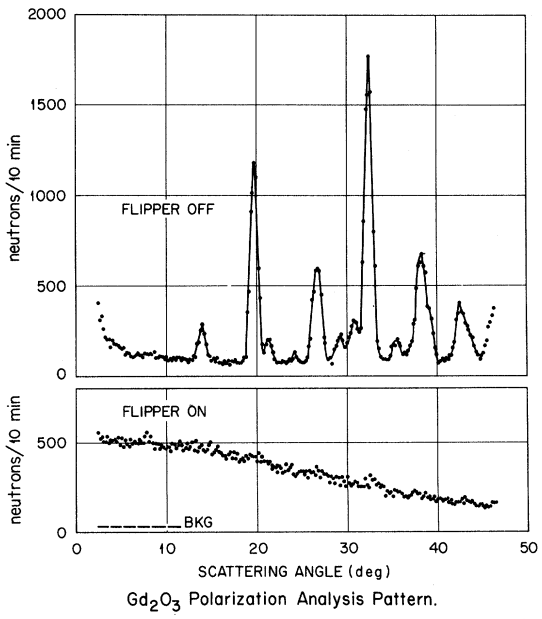

FIG. 14. Polarization-analysis pattern of $^{160}Gd_2O_3$. With the flipper off only coherent nuclear scattering is detected; with the flipper on, only paramagnetic scattering is detected. In a conventional experiment both types of scattering would be seen and the resulting pattern would be the sum of the two shown.

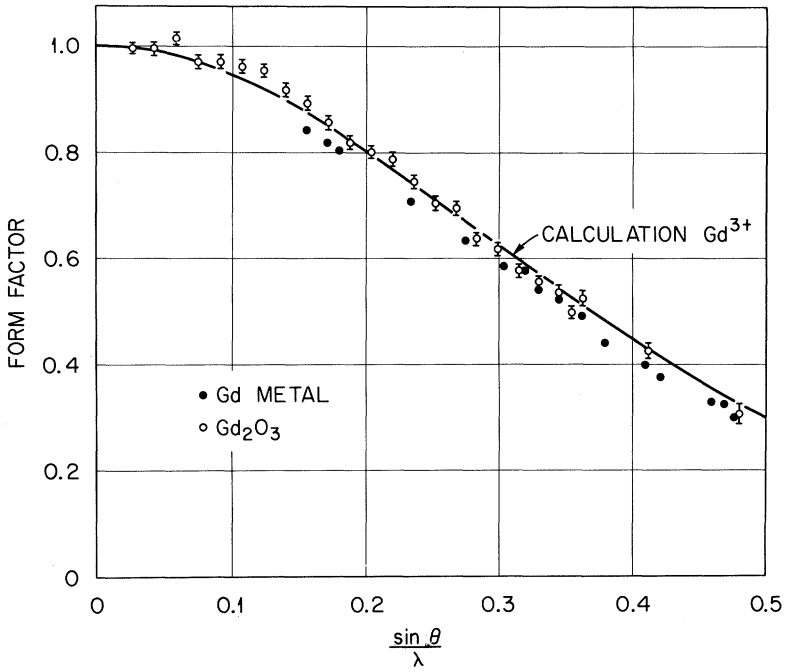

FIG. 15. Magnetic form factor of $^{160}Gd^{+3}$ as measured from $^{160}Gd_2O_3$. The solid line is the Blume-Freeman-Watson form factor. The closed circles show the experimental $4f$ form factor measured on the metal. Except for very small scattering angles the calculated form factor fits the experimental oxide form factor remarkably well.

separated in a logical manner into a local part and a diffuse part.

(ii) The diffuse part is long range and oscillatory, which are properties generally attributed to conduction-electron polarization. At the atomic sites this spin polarization is parallel to that of the local contribution.

(iii) The local part of the spin density is not in good agreement with nonrelativistic Hartree-Fock wave functions for the $4f$ electrons. The agreement is much better with a relativistic Hartree-Fock-Slater calculation using a reasonable value for the Slater-exchange coefficient.

(iv) The shape of the total spin density is the same within experimental error at 96 and 313 °K. This is consistent with the assumption that the magnitude of the conduction-electron spin polarization is proportional to the average value of the z component of the local moment. We do not yet conclude that this assumption is good at all temperatures.

(v) The metallic local form factor is different than the paramagnetic form factor of Gd_2O_3. The results indicate that the $4f$ electrons in the oxide are more compact than in the metal. Accepting the theoretical conclusion of Davis and Cooke that screening by conduction electrons has a very small influence on the $4f$ wave functions, this difference between the metal and oxide is not understood.

ACKNOWLEDGMENTS

The authors are grateful to Dr. George Rogosa of the USAEC for authorizing the separation of high-isotopic-purity gadolinium, to the Stable Isotopes Division of ORNL for doing it, to Dr. D. E. LaValle for producing the metal, to Dr. A. H. Millhouse for growing the crystal, and to Mr. James Sellers for technical assistance.

APPENDIX

In this Appendix we describe the data-reduction process, including the determination of experimental correction parameters and error analysis. A method of interpreting the flipping ratio in the presence of imperfect beam polarization, imperfect flipping, $\frac{1}{2}\lambda$ contamination and low secondary extinction has been previously described.[15] We wish to extend this treatment by also including corrections for sample depolarization and spin-flip scattering.

In the usual treatment of secondary extinction, a solution is sought for a set of two linear differential equations describing the interchange of intensity between the incident and reflected beams. In a polarized-beam experiment, when depolarization or spin-flip scattering may be important, it is necessary to deal with a set of four differential equations describing the change of intensity of both spin components in both beam directions. We characterize the sample by a set of linear reflectivity coefficients $r_{ij}^{ss'}$ which give the probability per unit path length for reflection from beam i to beam j with change of spin state from s to s'. The subscripts can take the values 0 or 1 for incident or reflected beam directions, and the superscripts can take the values + or −. In this notation, a depolarization process in the incident beam would be

characterized by r_{00}^{+-}.

We consider a crystal in the shape of a flat plate which is large compared to the incident-beam cross section, with the reflected beam in transmission geometry. The following differential equations describe the change in power (neutrons/sec) in the various beams as they traverse a crystal layer of thickness dx at depth x below the surface:

$$\frac{dN_i^s}{dx} = r_{ji}^{ss}\gamma_j N_j^s + r_{ji}^{s's}\gamma_j N_j^{s'} + r_{ii}^{s's}\gamma_i N_i^{s'} - r_{ij}^{ss}\gamma_i N_i^s - r_{ij}^{ss'}\gamma_i N_i^s - r_{ii}^{ss'}\gamma_i N_i^s - \mu_a \gamma_i N_i^s , \quad \text{(A1)}$$

where N_i^s is the power in spin state s of beam i, γ_i is the reciprocal of the absolute value of the direction cosine of beam i relative to the normal to the crystal surface, and μ_a is the linear absorption coefficient.

We wish to solve the set of four coupled equations given by Eq. (A1) subject to the boundary conditions $N_1^+(0) = N_1^-(0) = 0$. The experiments were always performed under conditions of low extinction, low depolarization, and low absorption, so we will seek an approximate solution which is valid in the limit $r_{ij}^{ss'} l_i \ll 1$ and $\mu_a l_i \ll 1$, where l_i is the path length of beam i. If T is the crystal thickness, $l_i = \gamma_i T$. We follow the procedure of Moon and Shull,[17] obtaining $N_1^+(T)$ and $N_1^-(T)$ as Taylor-series expansions about the point $x = 0$, keeping terms up to the second order. In this experiment the detector is not polarization sensitive, so we are interested in the quantity $N_1(T) = N_1^+(T) + N_1^-(T)$. We assume that the scattering processes are reversible,

$$r_{01}^{ss'} = r_{10}^{ss'} = r^{ss'} , \quad \text{(A2)}$$

that the spin-flip scattering is independent of the initial spin state,

$$r_{ij}^{+-} = r_{ij}^{-+} , \quad \text{(A3)}$$

and that the depolarization is independent of the beam direction and initial spin state,

$$r_{00}^{+-} = r_{00}^{-+} = r_{11}^{+-} = r_{11}^{-+} = \mu_d . \quad \text{(A4)}$$

For the total reflected power, we obtain

$$N_1 = l_0\{r^+ N_0^+ + r^- N_0^- - \tfrac{1}{2}[r^{+2}(l_0 + l_1)N_0^+ + r^{-2}(l_0 + l_1)N_0^-] + \tfrac{1}{2}[(r^+ - r^-)l_1 r^{+-}(N_0^+ - N_0^-)] - \tfrac{1}{2}[(r^+ - r^-)\mu_d l_0 \times (N_0^+ - N_0^-)] - \tfrac{1}{2}\mu_a(l_0 + l_1)(r^+ N_0^+ + r^- N_0^-)\} , \quad \text{(A5)}$$

where

$$r^+ = r^{++} + r^{+-} \quad \text{(A6)}$$

and

$$r^- = r^{--} + r^{-+} . \quad \text{(A7)}$$

The first two terms in Eq. (A5) give the uncorrected reflected power. The terms inside the first square brackets give an extinction correction which is not quite valid if there is spin-flip scattering. The second square brackets enclose terms correcting the extinction terms to properly account for the spin-flip scattering, and finally there are corrections for depolarization and absorption. Using the definitions

$$r = \tfrac{1}{2}(r^+ + r^-) , \quad \text{(A8)}$$

$$P_x = (r^+ - r^-)/(r^+ + r^-) , \quad \text{(A9)}$$

$$N_0 = N_0^+ + N_0^- , \quad \text{(A10)}$$

$$P_0 = (N_0^+ - N_0^-)/N_0 , \quad \text{(A11)}$$

Eq. (A5) may be written as

$$N_1(P_0, P_x) = r l_0 N_0 [1 + P_0 P_x - \tfrac{1}{2} r(l_0 + l_1)(1 + 2P_0 P_x + P_x^2) + r^{+-} l_1 P_0 P_x - \mu_d l_0 P_0 P_x - \tfrac{1}{2}\mu_a(l_0 + l_1)(1 + P_0 P_x)] . \quad \text{(A12)}$$

The quantity r is the reflectivity for an unpolarized beam. For the $\frac{1}{2}\lambda$ component, we neglect the correction terms, so that

$$N_1^h(P_0^h, P_x^h) = r^h l_0 N_0^h (1 + P_0^h P_x^h) . \quad \text{(A13)}$$

With the flipper off, the total reflected beam power is given by

$$N^{off} = N_1(P_0, P_x) + N_1^h(P_0^h, P_x^h) , \quad \text{(A14)}$$

and with the flipper on, by

$$N^{on} = N_1(-P_0 P_f, P_x) + N_1^h(0, P_x^h) , \quad \text{(A15)}$$

where use is made of the fact that a flipper tuned to optimize the flipping efficiency at wavelength λ will depolarize the $\frac{1}{2}\lambda$ component. The observed flipping ratio is given by

$$R = N^{off}/N^{on} . \quad \text{(A16)}$$

We choose to calculate a related quantity

$$P_x' \equiv \frac{R-1}{R+1} = \frac{N^{off} - N^{on}}{N^{off} + N^{on}} . \quad \text{(A17)}$$

We wish to obtain an expression for P_x in terms of P_x'. Performing the indicated substitutions and solving for P_x, we obtain

$$P_x = P_x'[1 + 2(\delta_0 + \delta_f) + \delta_f(P_x' - 1) + \delta_h + \tfrac{1}{2} r(l_0 + l_1)(1 - P_x'^2) - l_1 r^{+-} + \mu_d l_0] , \quad \text{(A18)}$$

where

$$\delta_0 = \tfrac{1}{2}(1 - P_0) , \quad \text{(A19)}$$

$$\delta_f = \tfrac{1}{2}(1 - P_f) \quad \text{(A20)}$$

$$\delta_h = \frac{r^h}{r}\frac{N_0^h}{N_0}\left(1 + \frac{P_x' - 1}{2P_x'} P_0^h P_x^h\right) . \quad \text{(A21)}$$

In obtaining Eq. (A18), we have retained only the first-order correction terms. Although Eq. (A18)

has been derived for the case where the reflected beam is in transmission geometry, it can be shown that the same equation applies to the case of reflection geometry in the thin-crystal limit. This is the basic equation used in correcting the data. The terms in δ_0, δ_f, and δ_h arise from instrumental imperfections, while the last three terms correct for extinction, spin-flip scattering, and depolarization within the sample.

In the evaluation of the reflectivities, we assume the crystal has a Gaussian mosaic distribution function and we evaluate the peak reflectivity. The reflectivities are given by

$$r^{++} = G(b + pq^2)^2 , \tag{A22}$$

$$r^{--} = G(b - pq^2)^2 , \tag{A23}$$

$$r^{+-} = r^{-+} = Gp^2q^2(1 - q^2) , \tag{A24}$$

where

$$G = [(2\pi)^{1/2}\eta]^{-1}\lambda^3 N^2 F_G^2/\sin 2\theta . \tag{A25}$$

Here λ is the wavelength, N is the number of unit cells per unit volume, F_G is the geometric structure factor, 2θ is the scattering angle, and η is the mosaic distribution parameter. The quantity q^2 is the square of the angle between the magnetization vector and the scattering vector, and is readily calculated from the orientation of the magnetic field. In our experiments $q^2 \approx 1$, so that the spin-flip scattering was always very small. The total reflectivity which enters in the extinction correction term is given by

$$r = G(b^2 + p^2q^2) . \tag{A26}$$

Finally, we have that

$$P_x = \frac{2bpq^2}{b^2 + p^2q^2} , \tag{A27}$$

from which the desired ratio of magnetic to nuclear amplitudes may be obtained:

$$\frac{p}{b} = \frac{1}{P_x} \pm \left(\frac{1}{P_x^2} - \frac{1}{q^2}\right)^{1/2} . \tag{A28}$$

Let us turn now to the determination of the various parameters which enter the correction terms of Eq. (A18). The determination of the beam polarization and flipping efficiency can be achieved by making separate measurements of the "shim ratio" and flipping ratio with an analyzing crystal at the test position.[38] However, we note from Eq. (A18) that it is the combination $(\delta_0 + \delta_f)$ which is the most important instrumental correction. These corrections are appreciable when $P_x' \approx 1$ $(p/b \approx 1)$, but in this case the term $\delta_f(P_x' - 1)$ becomes very small. We have, therefore, not attempted to make accurate measurements of δ_f, but have concentrated on measuring $(\delta_0 + \delta_f)$. The customary technique is to measure the flipping ratio using an analyzer at the test position. The inverse flipping ratio is given by

$$\frac{1}{R} = \frac{1 - P_0P_fP_A}{1 + P_0P_A} \simeq \delta_0 + \delta_f + \delta_A , \tag{A29}$$

where $P_A = 1 - 2\delta_A$ is a measure of the polarizing efficiency of the analyzer. The difficulty in this technique is that δ_A is usually not known and the assumption is frequently made that $\delta_A = \delta_0$. We have avoided this difficulty by using two analyzing crystals with the second analyzer set to give Bragg reflection of the reflected beam off the first analyzer. This results in a nearly perfect analyzing system. If δ_A for one crystal is about 10^{-2}, then the corresponding number for the double analyzer will be about 10^{-4}. The inverse flipping ratio for the double analyzer is

$$\frac{1}{R} = \frac{1 - P_0P_fP_{A1} - P_0P_fP_{A2} + P_{A1}P_{A2}}{1 + P_0P_{A1} + P_0P_{A2} + P_{A1}P_{A2}} \simeq \delta_0 + \delta_f . \tag{A30}$$

Taking care to sample the same part of the beam that is incident on the test crystal, we have used this double-analyzer technique to determine $(\delta_0 + \delta_f)$ at the various wavelengths used in these experiments. Flipping ratios as high as 430 were measured in this way. In evaluating the third term of Eq. (A18), we took advantage of the insensitivity of the final result to this term and used

$$\delta_f = \tfrac{1}{2}(\delta_0 + \delta_f) \pm \tfrac{1}{2}(\delta_0 + \delta_f) . \tag{A31}$$

The scale of the $\frac{1}{2}\lambda$ correction is set by the factor N_0^h/N_0 in Eq. (A21), which is the ratio of incident intensities in the $\frac{1}{2}\lambda$ and λ components. This ratio was determined by measuring the integrated intensity for the same reflection from the same crystal for both wavelength components. At $\lambda = 1.07$ Å this ratio was 0.0088. From the work of Nathans and Paoletti,[39] we obtain $P_0^h = 0.53$. The factor r^h/r was calculated using Eqs. (A25) and (A26), and approximate values of P_x^h were calculated assuming the validity of the free-ion form factor.

The extinction and spin-flip scattering corrections depend on the mosaic width parameter η, which was determined by measuring the width of the rocking curve using a sharp Ge crystal with matched d spacing as a monochromator. The value of η determined in this manner may not be the proper value for insertion in the reflectivity calculation if the mosaic distribution shows variations within the volume of the crystal. In addition, by evaluating the mosaic distribution at its peak value, we are really assuming that the instrumental resolution is narrow compared to the mosaic distribution. This is not a particularly good assumption. Therefore, we should not expect the extinction correction to be more than a rough approximation, which is adequate if the correction is sufficiently small. Be-

cause of the approximate nature of the extinction and spin-flip–scattering corrections, no attempt was made to accurately calculate the effective path lengths of the incident and reflected beams. An average path length for a particular crystal was used for all reflections with an error assigned which was large enough to include both the shortest and longest possible path lengths.

As discussed in the main text, we used two techniques to measure the sample depolarization. In the polarization transmission measurement, the change in flipping ratio of an analyzing crystal is observed when the sample is inserted before the analyzer. The difference in the inverse flipping ratio is

$$\frac{1}{R_{\text{in}}}-\frac{1}{R_{\text{out}}}\cong 2\mu_D l_0 \ . \tag{A32}$$

This experiment is rather difficult to perform with very small crystals mounted in a cryostat, because the beam must be reduced in size so that all of the neutrons pass through the test crystal. In the other method of measuring depolarization, we make an analyzer out of the test crystal itself by varying the temperature until $p/b=1$. The difficulty is that the depolarization measurement is made at the wrong temperature. To compare with the polarization transmission results, we assumed that the depolarization had the same temperature dependence as the magnetization. The dependence of the incident-beam path length on the scattering angle was taken into account in evaluating the depolarization correction term in Eq. (A18).

The difficulty in determining errors in the final value of p/b has been discussed by Kendrick *et al.*[40] We have followed a scheme similar to theirs. We rewrite Eq. (A18) as

$$P_x=P_x'+\sum_{i=1}^{6} C_i \ , \tag{A33}$$

where the C_i stand for the six correction terms. The error in P_x was calculated as

$$\Delta P_x=(\Delta P_x'^2+\textstyle\sum_i \Delta C_i^2)^{1/2} \ . \tag{A34}$$

The individual ΔC_i were based on errors in the parameters discussed in the preceding paragraphs. Some of these errors are statistical but some are uncertainties expressing our ignorance. The error in P_x' is definitely statistical. Each of the 350 flipping-ratio measurements is the mean of 20 identical experiments with counting times optimized to result in the lowest statistical error in the ratio. The standard deviation from this mean was calculated by computing the root-mean-square deviation of the 20 observations and comparing with the standard deviation computed from the total number of counts recorded, assuming Poisson statistics. These two standard-deviation computations were always in excellent agreement. If the function on the right-hand side of Eq. (A28) is defined as $H(P_x)$, then the error in p/b was computed as

$$\Delta p/b=\tfrac{1}{2}[H(P_x+\Delta P_x)-H(P_x-\Delta P_x)] \ . \tag{A35}$$

The number of independent measurements using different wavelengths, different crystals, or different, but equivalent, reflections varied from 1 to 16. In general, the calculated errors gave a good measure of the spread in observed p/b values.

The entire data-reduction process was performed by a computer program. In addition to the final p/b value and associated error, the importance of each of the correction terms was displayed by calculating the quantities

$$\Delta_i=H(P_x'+C_i)-H(P_x') \ . \tag{A36}$$

It is these quantities which are shown in Table II.

---

†Research sponsored by the U. S. Atomic Energy Commission under contract with Union Carbide Corp.

[1]H. E. Nigh, S. Legvold, and F. H. Spedding, Phys. Rev. 132, 1092 (1963).

[2]W. D. Corner, W. C. Roe, and K. N. R. Taylor, Proc. Phys. Soc. (London) 80, 927 (1962).

[3]C. D. Graham, J. Phys. Soc. Japan 17, 1310 (1962).

[4]J. W. Cable and E. O. Wollan, Phys. Rev. 165, 733 (1968).

[5]See, for example, R. M. Moon, Phys. Rev. 136, A195 (1964); H. A. Mook, *ibid.* 148, 495 (1966); C. G. Shull and H. A. Mook, Phys. Rev. Letters 16, 184 (1966). Reviews are given by A. Paoletti, in *Proceedings of the Symposium on Current Problems in Physics, Casaccia, September*, 1968 (Comitato Nazionale Energia Nucleare, Milan, 1970) pp. 151–183; R. M. Moon, Kjeller Report No. KR-132, 1968, pp. 239–245 (unpublished).

[6]O. Steinsvoll, G. Shirane, R. Nathans, M. Blume, H. A. Alperin, and S. J. Pickart, Phys. Rev. 161, 499 (1967).

[7]T. O. Brun and G. H. Lander, J. Phys. 32, 571 (1971).

[8]T. O. Brun and G. H. Lander, Phys. Rev. Letters 23, 1295 (1969).

[9]W. C. Koehler, R. M. Moon, J. W. Cable, and H. R. Child, J. Phys. 32, 296 (1971).

[10]R. M. Moon, W. C. Koehler, J. W. Cable, and H. R. Child, J. Appl. Phys. 42, 1303 (1971).

[11]R. M. Moon and W. C. Koehler, Phys. Rev. Letters 27, 407 (1971).

[12]H. E. Nigh, J. Appl. Phys. 34, 3323 (1963).

[13]F. J. Darnell, Phys. Rev. 130, 1825 (1963).

[14]In this analysis it is assumed that the nuclear and magnetic temperature correction factors are equal. See the section on high-temperature measurements below.

[15]R. M. Moon, MIT Lincoln Laboratory Technical Report No. 312, 1963 (unpublished); Phys. Rev. 136, A195

(1964).

[16]Actually, what enters most significantly in the corrections is the combination of deviations from perfection in P_0 and P_f. The individual figures of merit are given here for general interest. See the Appendix.

[17]R. M. Moon and C. G. Shull, Acta Cryst. 17, 805 (1964).

[18]A. J. Blodgett, Jr., W. E. Spicer, and A. Y-C. Yu, in *Optical Properties and Electronic Structures of Metals and Alloys*, edited by F. Abelès (North-Holland, Amsterdam, 1966), p. 247.

[19]H. R. Child, R. M. Moon, L. J. Raubenheimer, and W. C. Koehler, J. Appl. Phys. 38, 1381 (1967).

[20]W. C. Koehler, E. O. Wollan, and M. K. Wilkinson, Phys. Rev. 110, 37 (1958).

[21]A. Fert, Bull. Soc. Franc. Mineral. Crist. 85, 267 (1962).

[22]R. M. Moon, W. C. Koehler, H. R. Child, and L. J. Raubenheimer, Phys. Rev. 176, 722 (1968).

[23]L. Pauling and M. D. Shappell, Z. Krist. 75, 128 (1930).

[24]M. Blume, A. J. Freeman, and R. E. Watson, J. Chem. Phys. 37, 1245 (1962); 41, 1874 (1964).

[25]A. J. Freeman and R. E. Watson, Phys. Rev. 127, 2058 (1962).

[26]An investigation of the magnetic structure of Gd with a sample enriched to 98.6% ^{160}Gd has been reported. {V. M. Kuchin, V. A. Semenkov, S. Sh. Shil'shtein, and Yu. B. Patrikeev, Zh. Eksperim. i Teor. Fiz. 55, 1241 (1964) [Sov. Phys. JETP 28, 649 (1969)].} They conclude, in agreement with other investigations, that gadolinium is a normal ferromagnet at all temperatures below T_c, and that the direction of magnetization varies with temperature in a complex way (Refs. 2–4). Their conclusion that the distribution of spin density in metallic gadolinium agrees well with that calculated for the trivalent ion is not supported by this investigation. We believe the discrepancy is due to the inherently smaller precision of the unpolarized-beam method compared to the polarized-beam techniques, to the large number of parameters which they required for the reduction of their data, and to the high absorption in their specimen.

[27]R. M. Moon, Intern. J. Magnetism 1, 219 (1971).

[28]W. C. Koehler and E. O. Wollan, Phys. Rev. 92, 1380 (1953).

[29]G. T. Trammell, Phys. Rev. 92, 1387 (1953).

[30]T. O. Brun, G. H. Lander, and G. P. Felcher, Bull. Am. Phys. Soc. 16, 325 (1971).

[31]H. Davis and J. Cooke, A.I.P. Conference Proceedings Series 1972 (unpublished).

[32]C. W. Nestor *et al.*, Oak Ridge National Laboratory Report No. ORNL-4027, 1966 (unpublished).

[33]R. E. Watson and A. J. Freeman, Phys. Rev. Letters 6, 277 (1961).

[34]R. E. Watson (private communication).

[35]R. E. Watson, S. Koide, M. Peter, and A. J. Freeman, Phys. Rev. 139, A167 (1965).

[36]Jun Kondo, Progr. Theoret. Phys. (Kyoto) 28, 846 (1962).

[37]R. M. Moon, T. Riste, and W. C. Koehler, Phys. Rev. 181, 920 (1969).

[38]R. Nathans, C. G. Shull, G. Shirane, and A. Anderson, J. Phys. Chem. Solids 10, 138 (1959).

[39]R. Nathans and A. Paoletti, Phys. Rev. Letters 2, 254 (1959).

[40]H. Kendrick, S. A. Werner, and A. Arrott, Nucl. Instr. Methods 68, 50 (1969).

PHYSICAL REVIEW B VOLUME 5, NUMBER 3 1 FEBRUARY 1972

Attenuation of Low-Energy Electrons by Solids: Results from X-Ray Photoelectron Spectroscopy*

R. G. Steinhardt
Hollins College, Virginia 24020 *and Brookhaven National Laboratory, Upton, New York* 11973

and

J. Hudis and M. L. Perlman
Chemistry Department, Brookhaven National Laboratory, Upton, New York 11973

(Received 9 August 1971)

The scattering half-thickness for electrons has been experimentally determined to be ≈ 0.25 $\mu g/cm^2$ (≈ 13 Å carbon) for 1169-eV electrons and ≈ 0.21 $\mu g/cm^2$ (≈ 10 Å carbon) for 920-eV electrons. The corresponding mass-scattering coefficients are 2.75 ± 0.19 and 3.32 ± 0.37 $cm^2/\mu g$. Other useful and related attenuation parameters are defined and calculated. These results were obtained from measurements of the attenuation by thin carbon films (5–60 Å) of monoenergetic photoelectrons originating from gold substrates irradiated with Mg K_α x rays, and also from measurements of the concomitant increase in carbon photoelectron intensity. Scattering of electrons in the energy range about 1 keV is greater than has generally been indicated.

INTRODUCTION

The attenuation of low-energy electrons ($\approx$1000 eV) has become increasingly important because of the growing use of high-resolution x-ray photoelectron spectroscopy for investigations in solid-state physics and chemistry.[1] While it is clear that x-ray photoelectron spectroscopy yields in-